



seit 1558

Friedrich-Schiller-Universität Jena
Biologisch-Pharmazeutische Fakultät

Functional manipulation of insect odorant receptors via co-receptor mutation

Diplomarbeit

Zur Erlangung des akademischen Grades eines
Diplom-Biologen



MAX-PLANCK-GESELLSCHAFT

angefertigt am
Max-Planck-Institut für chemische Ökologie
Abteilung Evolutionäre Neuroethologie

vorgelegt von
Kerstin Pasemann
geboren am 23. Juni 1984 in Salzwedel

Jena, November 2011

Gutachter:

PD Dr. Dieter Wicher
Max-Planck-Institut für chemische Ökologie
Hans-Knöll-Strasse 8
07745 Jena

Prof. Dr. Bill Hansson
Max-Planck-Institut für chemische Ökologie
Hans-Knöll-Strasse 8
07745 Jena

Table of content

1. Introduction	1
1.1 Studying an insect's nose	1
1.2 Anatomy of the olfactory system in <i>Drosophila melanogaster</i>	1
1.3 Odorant receptors	3
1.4 Controversy in signal transduction	4
1.5 Objective of the present work	7
2. Material and Methods	9
2.1 Material	9
2.1.1. Cell lines	9
2.1.2 Solutions for patch-clamp-experiments	10
2.1.3 Buffer for immunofluorescence	11
2.1.4 Chemicals	11
2.1.5 Media (cell culture)	12
2.1.6 Materials	12
2.1.7 Equipment	13
2.1.8 Software	13

2.2 Methods	14
2.2.1 Cell culture	14
2.2.2 Patch-Clamp-technique	15
2.2.3 Immunofluorescence	18
3. Results	19
3.1 Comparison of ionotropic and metabotropic current in Orco GYG transfected HEK-cells	19
3.2 Permeability ratios for Orco PKC	21
3.3 Orco single channel currents	21
3.3.1 Determination of single-channel currents via amplitude histograms	21
3.3.2 Determination of single-channel currents via variance analysis	23
3.3.2 Concentration dependence	26
3.4 Characterization of the transfection via immunofluorescence	27
3.4.1 Confocal micrographs	27
3.4.2 Membrane insertion of OR proteins	29
4. Discussion	32
4.1 Insect ORs form two pore channels	32
4.2 PKC mediated phosphorylation does not affect Orco permeability	33
4.3 Orco single channel current	33

4.3 Current model of insect olfactory receptor signal transduction	35
5. Summary	37
6. Acknowledgement	38
7. References	39
8. Abbreviations	42
9. Declaration of academic integrity	44

1. Introduction

1.1 Studying an insect's nose

The perception of odorants is the most complex chemical sense owed to its diversity and combinatority. The detection of chemical cues in the environment enables animals to identify beneficial resources like food, dangerous substances, intraspecific signals and opponents. Emphasizing the general importance to animals the sense of smell is supposed to be the most ancient sense in animals (Strausfeld & Hildebrand 1999). So animals have evolved a complex collectivity of odorant receptors for perception of volatile molecules. Due to its complexity the understanding of olfaction is challenging, this asks for a facilitated approach to olfactory circuitry in a simpler system than vertebrate olfactory systems. The investigation of the model organism *Drosophila melanogaster* is suggesting as it also represents insects - the richest taxa in fauna (Grimaldi & Engel 2005). Recent molecular and neuroanatomical research has yielded an almost complete description of chemosensory peripheral neuroanatomy and its function in *Drosophila* (Vosshall & Stocker 2007). At first sight the nose of an insect seems to have nothing in common with vertebrates, but the morphological organization of olfactory sensory neurons (OSN) is quite similar. To enlarge upon anatomy the next chapter describes more precisely the olfactory organs in adult flies.

1.2 Anatomy of the olfactory system in *Drosophila melanogaster*

Flies perceive odors with their olfactory organs, the third segment of the antenna and the maxillary palp are the main olfactory sensory organs. The surface of these sensory appendages is covered with olfactory sensilla, varying in size, morphology and substance specificity. These sensilla are classified in three major types: basiconic, coeloconic and trichoid (Figure 1). Basiconic sensilla are distributed at the medial-proximal part of the 3rd segment and house receptors for CO₂ and general odorants (Vosshall & Stocker 2007). Pheromones detecting trichoid sensilla are located at medial-proximal side of the

antenna. Between these edges coeloconic sensilla are found that express no conventional receptors but the recently discovered family of ionotropic receptors (IR) (Benton et al 2009). This odorant receptor family is related to ionotropic glutamate receptors and detects amines and acids (Silbering et al 2011, Yao et al 2005).

Altogether all sensilla house around 1200 olfactory sensory neurons (OSN), each sensillum contains one to four OSN, which are backed up physiologically and isolated from other nearby OSNs by surrounding support cells (Vosshall & Stocker 2007). The dendrites of the bipolar OSN extend into a shaft filled with sensillum lymph, which is structured through its outer porous cuticle (Figure 1C). Odor molecules pass this permeable covering and cross sensillum lymph to the exposed dendrites of the OSN. Odorant binding proteins are involved in the transport through lymph, especially for hydrophobic odorants (Carey & Carlson 2011, Vogt & Riddiford 1981). All OSN axons bundle into the antennal nerve, it projects along with auditory fibers from the second antennal segment and the arista into the antennal lobe. OSN on the maxillary palp are organized more facile. Housed pair wise in around 60 basiconic sensilla these 120 neurons project into the antennal lobe (AL) fasciculating with gustatory neurons (Naresh Singh & Nayak 1985).

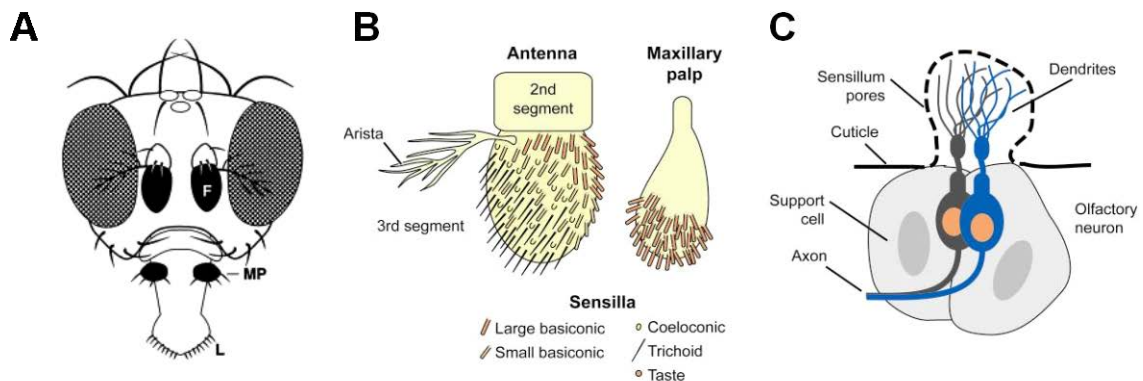


Figure 1 Morphology of the olfactory system in insects **A** Head of an adult male vinegar fly, *Drosophila melanogaster* (frontal). The antenna is connected to the funiculus (F). Abbreviations: Maxillary palp (MP) Labellum (L) **B** Distribution of sensilla types for the 3rd antennal segment and maxillary palps **C** Schematic structure of a sensillum hosting two OSN. Figure merged from (Shanbhag et al 1999) and (Vosshall & Stocker 2007)

The AL, which receives the input from the OSN, consists of 43 morphologically defined glomeruli. These glomeruli are spherical structures of densely packed neuropil. According to the number of ORs expressed in adults it was assumed that one OR projects into one specific glomerulus (Gao et al 2000, Vosshall et al 2000). Moreover, projections from the three antennal sensilla types and the basiconic palp sensilla distribute as spatial cluster in the AL: similar receptors tend to map to proximate glomeruli (Couto et al 2005). Initial horizontal modulation of chemosensory information can be realized among glomeruli by GABAergic local interneuronal connections (Wilson & Laurent 2005). From these primary centers the olfactory information is processed via cholinergic projection neurons into higher brain centers, the mushroom bodies and the lateral horn. The mushroom bodies are conceived as integrative center playing a role in learning and memory (Heisenberg 1998).

The olfactory system of this classic model organism consists of fractions of cells compared to vertebrates. The repertoire of odorant receptors, for which there are 60 OR genes, and the number of odorant receptor neurons are considerably smaller, thus enabling diverse genetic manipulation and simplifying its research.

1.3 Odorant receptors

First *Drosophila* ORs were spotted in 1999 via bioinformatic approaches searching for gene families with seven transmembrane domains, which are only expressed in OSNs (Clyne et al 1999, Gao & Chess 1999, Vosshall et al 1999). Transcribed from 60 genes, 62 ORs are currently known. Compared to the vertebrate G-protein coupled receptors insect ORs are inverted in membrane, hence they are regarded as a novel family that evolved independently (Benton et al 2006). The majority of OSN expresses two different receptor proteins: one conventional ligand-binding OR and the co-receptor Orco, which is expressed in virtually all fly OR sensory neurons (Krieger et al 2003).

Investigation on the interaction of these two receptors reports that null mutant flies without ubiquitous Orco showed behavioral and electrophysiological deficits to many different odors, suggesting that Orco associates with the conventional OR for signaling (Larsson et al 2004). Expressed separate in a heterologous cell system, the response of

conventional ORs was reduced crucially compared to cells with Orco co-expressed. This finding proposes that they form a heteromeric complex for signaling (Neuhaus et al 2005). Furthermore, Orco already associates with the conventional OR in the endomembrane system of the OSN and is needed for OR membrane trafficking and localization in basiconic and trichoid sensilla (Benton et al 2006, Larsson et al 2004). There is no hint that Orco is directly involved in odor recognition (Elmore et al 2003), attributing Orco to function as chaperone co-receptor.

1.4 Controversy in signal transduction

Following the receptor structure with seven transmembrane domains, a prolonged, G-protein coupled pathway is plausible. In contrast to expectations two studies could describe a fast ionotropic response, which is presumably caused by heteromeric ligand-gated ion channels (Sato et al 2008, Wicher et al 2008). The paper from Sato and colleagues argues for a basic model, where the pore is shaped by the specific odorant binding receptor and Orco (Figure 2A). Additionally Wicher *et al.* could confirm a metabotropic pathway beside the ionotropic one. The stimulation of Or22a and Orco coexpressed in a heterologous cell system, namely HEK293 cells, resulted in non-selective cation currents. These currents are activated by an ionotropic and a metabotropic pathway. In contrast to the fast and short response via the ionotropic pathway the metabotropic response was slow and prolonged (Figure 2B). Through application of cyclic nucleotides (8-bromo-cAMP or 8-bromo-cGMP) currents were evoked in cells transfected with Orco alone, this suggests that Orco can be functional without a ligand-binding OR. Stimulation of Or22a via Etb initiates a channel opening generating a fast and short response and mediates the release of G_s proteins. Subsequent the adenylyl cyclase (AC) is activated indirectly via G_s -proteins and leads to increased cAMP levels. This succeeds in an opening of Orco and arouses a delayed non-selective cation current (Wicher et al 2008).

These opposing models are based on variant lines of evidence. Sato *et al.* report that the fast odor evoked currents include an extracellular calcium influx. Many intercellular signaling cascades contain G-protein coupled pathways, so they examined known second

messenger to investigate this pathway. They applied cAMP, cGMP and inositol-1,4,5-triphosphate (IP₃) and observed no response. Also U73122, a phospholipase inhibitor, did not influence Ca²⁺ level elicited by Orco and Or47a. Additionally they could not find any increase of intercellular cAMP. These results can lead to the conclusion that no G α_q neither a G α_s pathway is present. Providing the position of an absence of G-proteins general inhibitor GDP- β S provoked no decline of responses in cells with Or47a/Orco. Recently Yao and colleagues investigated the role of G α_q -proteins *in vivo* by applying RNA interference constructs, competitive peptides and active G α_q -proteins during single-sensillum recordings and could not approve a functional occurrence in odor sensing neurons (Yao & Carlson 2010).

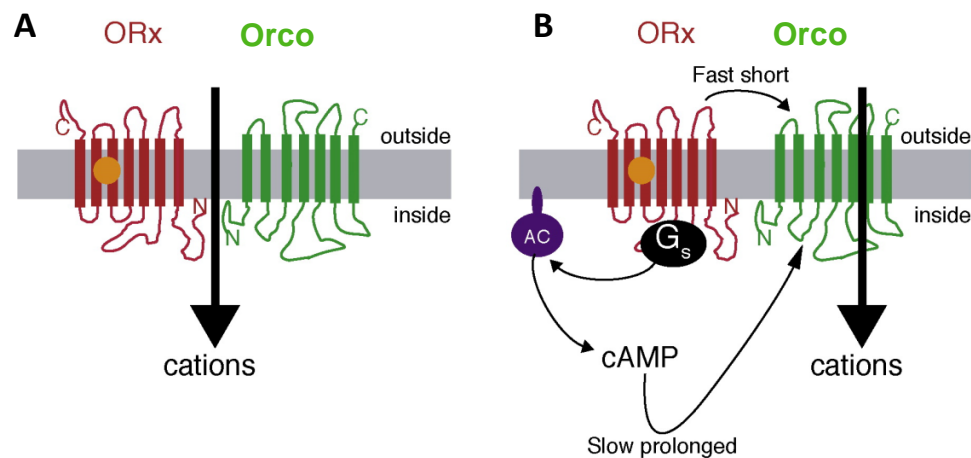


Figure 2 Models for olfactory signal transduction in insects from 2008 **A** Heteromeric ligand-gated cation channel activated rapidly; Or83b old term for Orco **B** Odor activated ionotropic (fast and slow) and metabotropic (slow and prolonged) pathway, involving G-proteins. Abbreviations: AC, adenylyl cyclase (Nakagawa & Vosshall 2009).

By contrast the study from Wicher and colleagues demonstrated a response of Orco to intercellular second messengers. The cyclic nucleotide analogues 8-bromo-cAMP and also 8-bromo-cGMP evoked currents in HEK293 cells transfected with Orco leading to the opposite interpretation. Also the general G-protein inhibitor GDP- β S diminished the sensitivity of the receptor complex. To prove an intracellular rise of cyclic nucleotides Or22a was co-expressed with human HCN2 or CNGA2 channels. The stimulation of Or22a with Etb resulted in a characteristic change of currents caused by these cyclic nucleotide gated ion channels and underpins a pathway via G α_s -protein. G α_s -proteins induce

activation of the AC, which is followed by an increase of the cyclic nucleotide level. Moreover the coexpression of G_s -activating adipokinetic hormone receptor (AKHR) and Orco induced currents after stimulation of AKHR. The shown metabotropic pathway was presumed that it functions as amplification system and enables the perception of low odorant concentrations (Wicher et al 2008). This position was confirmed by *in vivo* recordings: Deng et al. performed diverse experimental approaches focusing on G_{α_s} protein and proved the stimulatory effect of G_{α_s} proteins in olfactory signal transduction (Deng et al 2011).

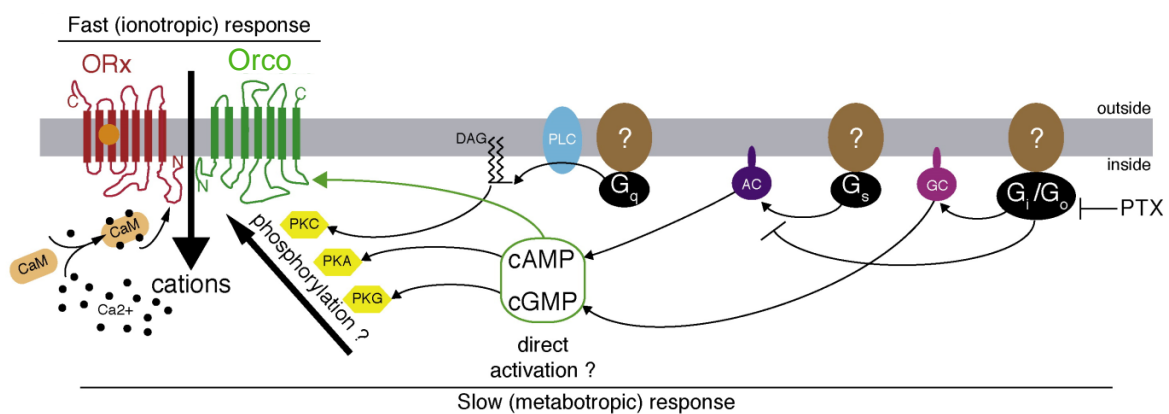


Figure 3 Integrative model from Nakagawa with the suggested variety of G-proteins. The ionotropic response is transduced via a heteromeric pore and a slow metabotropic response is proposed to be controlled by G-protein involving steps. Protein kinase A and G are phosphorylated by cAMP and cGMP whose levels are modulated by G_s and G_i/G_o . Protein kinase C can be influenced by the G_q -proteins dependent phospholipase C. Abbreviations: CaM calmodulin; PKC, protein kinase C; PKA, protein kinase A; PKG, protein kinase G; PLC, phospholipase C; AC, adenylate cyclase; GC, guanylate cyclase; PTX, pertussis toxin (Nakagawa & Vosshall 2009).

Subsequently a third model (Figure 3) was proposed, which combined both views (Nakagawa & Vosshall 2009). The shaping of the non-selective cation channel was hypothesized as heteromeric complex formation between OrX and Orco. This current is believed to get modulated by diverse G-protein cascades requesting especially a debate for G_s and G_q signaling. Recent work on an Orco mutant with altered phosphorylation sites showed a decline of responses in dependence of the degree of modification *in vitro*. Also single sensillum recordings influenced by microinjection of phospholipase C and protein kinase C inhibitors decreased the responsiveness *in vivo*. These results supply evidence

for involvement of G_q -proteins (Sargsyan et al 2011). A preceding study operating with genetically modified flies showed that $G\alpha_q$ proteins are required for an unreduced response in antennal neurons. These findings strengthen a supporting function of phospholipid intermediates in signal transduction (Kain et al 2008). An increasing number of studies could validate a metabotropic pathway so that the issue is moved to the question of accessory second messenger in downstream signaling. Furthermore, the three presented models differ in localization of the pore, so this needs further clarification together with specification of correspondent subunits of the OrX/Orco complex.

1.5 Objective of the present work

Relations between ionotropic and metabotropic response seem to be complex and it is not clear, how the ionotropic and metabotropic pathway are associated. In the present work experiments with a pharmacologically and genetically manipulation of receptor proteins in the metabotropic pathway were conducted to gain insights into the influence of Orco on the response. An Etb induced response in Or22a/Orco transfected HEK-cells is composed of an ionotropic and a metabotropic part. It has been shown that an odor-induced response can be evoked without G-proteins involved (Sato et al 2008, Yao & Carlson 2010). On the other hand, it was possible to induce the metabotropic response via second messengers in HEK-cells without any conventional receptors (Wicher et al 2008). This lead to the assumption that Orco can form a channel solitary. In this context it was tried to determine, if one or two pores are opened during a response. To corroborate the number of pores the GYG Orco mutant was coexpressed with Or22a and its Etb response compared to the wild type. GYG mutation was achieved by deletion of two residues in the TVVG~~YL~~G motif of Orco, which is similar to the TVGYG motif in K^+ -channels, presumed as a part of the selectivity filter. Excitation of Orco GYG showed a moderate inward rectification contrary to a slight outward rectification of Orco wild type and a reduced K^+ -permeability (Wicher et al 2008). Whole-cell recordings were conducted to test, if only the metabotropic component of the response is affected.

For further verification of a pathway via protein kinase C (PKC) an Orco PKC mutant was created by excluding five phosphorylation sites in Orco. Stimulation of the modified receptors revealed a severely reduced sensitivity to cAMP (Sargsyan et al 2011). To investigate altered ion selectivity as cause for the reduced response to cAMP the ion permeability of Orco PKC mutant was tried determine. Moreover the single channel conductance of coreceptor Orco was tried to define in inside-out-patches with a HEK293 related cell line. These T-Rex cells are considered to express lower levels of Orco, when transfected stable. Hence, with a low transfection rate a resolution of single channel currents might be achieved.

2. Material and Methods

2.1 Material

2.1.1 Cell lines

HEK293

For transfection of insect odorant receptors the HEK293 cell line was used, it was sourced from Dr. W. Dirks, DSMZ in Braunschweig, Germany. This cell line is based on a primary embryonic kidney cell culture transformed with adenovirus type 5.

T-Rex

Flp-In™-293 Cell Line, provided by Invitrogen Germany, was used for a stable expression of odorant receptors. This cell line was produced by transfecting HEK293 cells with a Flp-In™-vector, which expresses genes from a CMV promoter.

Plasmid DNA

pcDNA3(+)-Orco-GFP

pcDNA3.1(-)-OR22a

pcDNA3.1-Orco-GYG (cotransfected with EGFP)

pcDNA3.1(+/-)-Orco-PKC

2.1.2 Solutions for patch-clamp-experiments

Standard solutions

Standard external solution (SES)

chemical	concentration
KCl	5mM
NaCl	135mM
MgCl ₂ *6H ₂ O	1mM
HEPES	10mM
Glucose	10mM
CaCl ₂	1mM
pH 7,4 adjusted with NaOH/HCl	

Standard internal solution (SIS)

chemical	concentration
KCl	140mM
NaCl	4mM
MgATP	2mM
HEPES	10mM
EGTA	5mM
CaCl ₂	2,2mM
NaGTP	0,05mM
pH 7,3 adjusted with KOH/HCl	

The tested odorants were applied directly into the bath solution at the given concentration.

Solutions for permeability tests

Calcium external solution

chemical	concentration
NMDG	140mM
HCl	140mM
CaCl ₂	10mM
HEPES	15mM
Glucose	5mM
pH 7,4 adjusted with Tris/HCl	

Sodium external solution

chemical	concentration
NaCl	140mM
HEPES	15mM
Glucose	15mM
pH 7,4 adjusted with NaOH/HCl	

Sodium and calcium free compositions of the external solution were used for permeability tests.

2.1.3 Buffer for immunohistochemistry

Phosphate Buffered Saline (PBS)

chemical	concentration
NaCl	136mM
KCl	2,6mM
Na ₂ HPO ₄	10,1mM
KH ₂ PO ₄	1,7mM
pH 8,0 adjusted with HCl	

Blocking buffer

For all blocking steps in the immunohistochemical procedure normal goat serum (NGS) was added to the PBS for a 5%NGS /PBS blocking buffer. In some cases a detergent was needed, so Triton X-100 was added for a 5%NGS/0.1%TritonX/PBS blocking buffer.

2.1.4 Chemicals

Adenosine 5'-triphosphate magnesium salt	Sigma-Aldrich, Germany
Adenosine 3',5'-cyclic monophosphate	Sigma-Aldrich, Germany
8-bromoadenosine 3',5'-cyclic monophosphate	Sigma-Aldrich, Germany
Calcium chloride	Sigma-Aldrich, Germany
D-(+)-glucose	Sigma-Aldrich, Germany
EGTA (ethylene glycol tetraacetic acid)	Sigma-Aldrich, Germany
Ethanol	Carl Roth GmbH+Co. KG, Germany
Ethyl butyrate	Sigma-Aldrich, Germany
Formaldehyde	Sigma-Aldrich, Germany

GIBCO® HBSS	Invitrogen, Germany
HEPES	Sigma-Aldrich, Germany
Hydrogen chloride	Carl Roth GmbH+Co. KG, Germany
Isopropanol	Sigma-Aldrich, Germany
Potassium chloride	Carl Roth GmbH+Co. KG, Germany
Magnesium chloride	Carl Roth GmbH+Co. KG, Germany
Sodium chloride	Carl Roth GmbH+Co. KG, Germany
Sodium hydroxide	Carl Roth GmbH+Co. KG, Germany
Roti®FECT	Carl Roth GmbH+Co. KG, Germany
Sylgard 184	Dow Corning Corporation, USA
Triton-X-100	Sigma-Aldrich, Germany
W-7	Sigma-Aldrich, Germany
WGA coupled with Texas Red	Invitrogen, Germany

2.1.5 Media (cell culture)

Dulbecco-MEM	PAA Laboratories GmbH, Germany
Fetal bovine serum (FBS)	Invitrogen, Germany

2.1.6 Materials

Petri dishes	Greiner Bio-One GmbH, Germany
Culture flasks	Sarstedt, USA
Plastic pipettes (10ml)	Sarstedt, USA
Glass capillary	Hilgerber, Germany
Tissue Culture Plate 24	Sarstedt, USA
Cover slips (round)	neoLab Migge Laborbedarf, Germany

2.1.7 Equipment

Pneumatic PicoPump PV830	World Precision Instruments, USA
RSC-200	Biologic Science Instruments, France
Incubator HERAcCell 150	Heraeus Instruments, Germany
Fluorescence microscope AxioVert 200	Carl-Zeiss GmbH, Germany
Microscope Axioskop	Carl-Zeiss GmbH, Germany
Hot air blower HE 2300 Control	Mitabo, Tschechische Republik
Incubator	Heraeus Instruments, Germany
Laser module LSM 510	Carl-Zeiss GmbH, Germany
Mikroskop LSM 510 META	Carl-Zeiss GmbH, Germany
Mikroskop Axiovert 25	Carl-Zeiss GmbH, Germany
Micro forge MF-900	Narishige, Japan
Micromanipulator	Luigs & Neumann, Germany
Micropipette Puller P67	Sutter Instruments Co, USA
Millex [®] Syringe Driven Filter Unit	Millipore Corporation, USA
Millipore MilliQ Synthesis A10 Q-Guard [®] 2	Millipore Cooperation, USA
Patch-Clamp-Amplifier EPC9	HEKA-Elektronik, Germany
pH-Meter 766 Calimetric	Knick, Germany
Vortex/rotating Shaker VortexGenie 2	SI – Scientific Industries, USA
Binocular Stemi 2000	Carl-Zeiss GmbH, Germany
Vibration dampening table	NewPort, Germany
UV-lamp X-Cite Series 120	EXFO, Canada
Control module Micromanipulator SM-5	Luigs & Neumann, Germany

2.1.8 Software

GraphPad PRISM [®] 4	GraphPad Software, USA
MSOffice 2007	Microsoft Corporation, USA
IgorPro	WaveMetrics, Lake Oswego, USA

Heka Fitmaster	HEKA-Elektronik, Germany
Heka Patchmaster	HEKA-Elektronik, Germany
RSC-Software	Biologic Science Instruments, France
AxioCam-Software	Carl-Zeiss GmbH, Germany

2.2. Methods

2.2.1 Cell culture

HEK293 cells and T-Rex cells

HEK-293 cells and T-Rex cells were incubated at 37°C, at 100% humidity and 5% CO₂. The used culture medium consisted of one part Dulbeccos-MEM and one part FBS. To improve cell adherence especially pretreated standard culture flasks (T-75) were utilized. Cells are passaged regularly to prevent a proliferation stop resulting from confluence. At a confluence ratio of 80% the medium was completely removed from the culture flasks and washed with 10ml 37°C warm PBS-Medium. After removing the PBS medium 1ml Trypsine-EDTA was pipetted into the culture flask and spread onto the cell layer through swiveling the culture flask. After cells were dispersed, 5ml PBS medium was added. This suspension was centrifuged at 200xg for 5min and subsequently the supernatant was removed. The resulting cell pellet was absorbed; the cell density was determined and at a concentration of 2x10⁵ transferred to fresh standard culture flasks T-75.

Transfection

Cultivated cells (1 x 10⁵ cells) were plated onto gelatin covered lids of 35mm Petri dishes. These dishes were incubated at 37°C, 100% humidity and 5%CO₂ atmosphere for 24 hours. Two solutions for transfection were prepared containing 1µg pcDNA in 60µl culture medium and 5µl Rotifect in 60µl culture medium, which were mixed through pipetting up and down. After mixing the two solutions were combined for a transfection complex by pipetting up and down and incubating for 30minutes. The transfection

complex (125 μ l) was subsequently added to the cells that were held at 37°C in a CO₂ incubator with a 5%CO₂ atmosphere and humidity at 100%.

2.2.2 Patch-clamp-technique

The patch-clamp-technique is related to the voltage-clamp-methods (Hodgkin & Huxley 1952) and was described first in 1976 by Erwin Neher und Bert Sakmann. The voltage clamp is an ion channel current measurement, while the membrane voltage is fixed. It is based on the measurement of the compensating current and reflects changes of the membrane conductance depending inter alia on ion channels and ion transporters.

Patch-clamp technique allows the recording of small currents such as typical as in the range of single channels (Hamill et al 1981). Minimizing the leakage current between pipette and cell membrane reduces the background noise and allows recording of responses from single channels located in the cell membrane. This important progress in the field of electrophysiology is based on the development of extremely tight seals with a high resistance between pipette and membrane at the level of giga ohms.

Based on the *cell-attached* configuration all other configurations can be obtained (Figure 4). To obtain *whole-cell* configuration a piece of the cell membrane has to be pried out in the *cell-attached* mode by increased negative pressure in the tip of the capillary. In the *whole-cell* configuration the entire cytoplasm is accessed. With opening of the membrane an exchange between cytoplasm and pipette solution is proceeded, which usually implies a pipette solution with similar ion composition to cytoplasm. Follows a lifting of the patch pipette in *whole-cell* configuration, the *outside-out* configuration can be achieved. If this lift is already performed in *cell-attached* mode, an *inside-out* configuration can be the result. In this configuration the membrane is inverted and the glycocalyx is facing the pipette solution and the inner membrane surface is exposed to the bath solution. After obtaining a desired configuration an according stimulation can be recorded.

Performance of a patch-clamp-recording

The prepared Petri dishes, cultivated as described before, were inserted into a fitted holder on the stage of the fluorescence microscope Axiovert 200. By a fluorescence lamp X-Cite 120 and the corresponding filter GFP containing cells were identified. A pipette holder was attached to the pre-amplifier, wherein a glass electrode was fixed for patching the cell membrane. The pipette holder was attached to a micromanipulator, what enabled a precise movement. The electrical connection was performed via a chlorided silver wire, which is coated with Teflon except a little site near the top. As reference a silver-wire with Ag/AgCl pellet was dipped into the bath solution. For application of compounds Pneumatic PicoPump was installed and little amounts of solution were ejected into the bath solution by generating an overpressure in the filled glass pipettes.

Microscope and micromanipulators with all attachments were located on a vibration damping table and were surrounded by a faraday cage. All electronic devices inside the cage were grounded. The signals were acquired by the EPC9-amplifier, recorded and saved on the computer using the HEKA Patchmaster software.

Pulse protocols were programmed in Patchmaster software. For whole-cell recordings a current trace was recorded at -50 mV holding potential, in which a ramp protocol from -100 mV up to 100 mV was inserted every 200 ms. For inside-out experiments the patches were clamped on -60 mV holding potential and the current was acquired.

Analysis of data

Data were analyzed with Fitmaster and MSEXcel software. GraphPad and IgorPro software was used for graphic evaluation. Unless otherwise stated, data are given as mean and its standard deviation, n = number of cells/ patches.

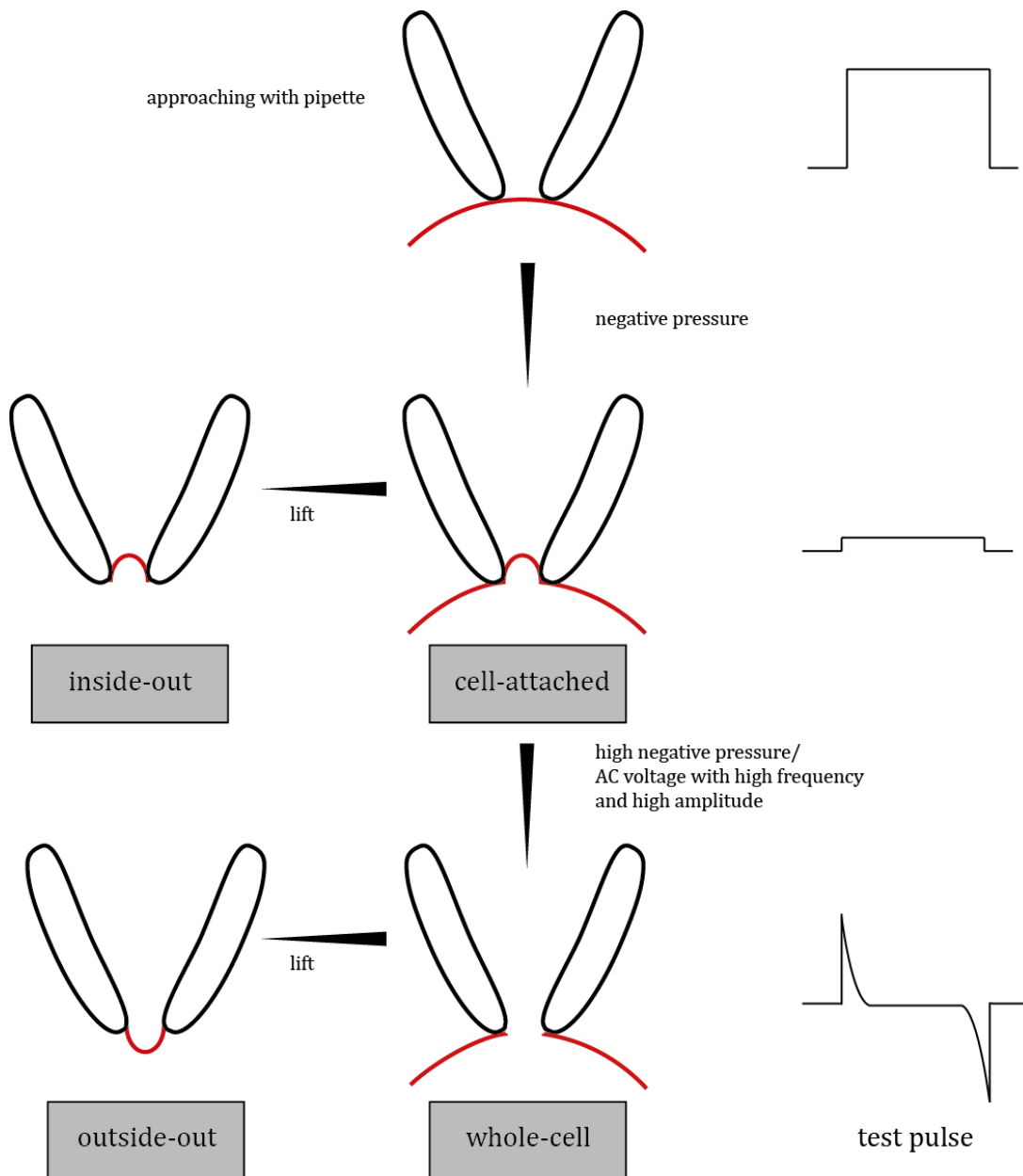


Figure 4 Patch-clamp configurations with its schematic test pulses (right column). When approaching the cell a little decrease in current indicates the contact with the cell membrane. Through negative pressure a cell-attached mode with a resistance of several gig ohms can be obtained. If this is succeeded the current in the test pulse is decreasing. By lifting the glass electrode the inside-out-configuration is feasible. A second negative pressure in *cell-attached*-configuration can lead to *whole-cell* configuration by a membrane breakthrough. In that case capacitive charging currents extend. Follows a lift of the glass electrode the *outside-out* mode can be achieved.

Permeability ratios for PKC were calculated with:

$$P_{\text{Na}} : P_{\text{K}} = [\text{K}^+]_{\text{i}} / [\text{Na}^+]_{\text{o}} \cdot \exp(V_{\text{rev}} F / RT)$$
$$P_{\text{Ca}} : P_{\text{K}} = [\text{K}^+]_{\text{i}} / 4[\text{Ca}^{2+}]_{\text{o}} \cdot \exp(V_{\text{rev}} 2F / RT)$$

P_{Ion} represents permeability of the according ion, $[\text{Ion}]_{\text{i}}$ und $[\text{Ion}]_{\text{o}}$ are the internal and external concentration of the respective ion, V_{rev} is the reversal potential, F is the Faraday constant, R is the gas constant and T is the absolute temperature.

2.2.3 Immunofluorescence

For staining via antibodies HEK293 cells were plated on poly-l-lysine coated cover slips and cultivated in a tissue culture plate. Formaldehyde solved at 4% in PBS was used for fixation of cells at 37°C for 1 min. Then the cover slips with adherent cells were washed in HBSS several times. Cell membrane was stained by a solution of WGA-conjugate combined with Texas Red (25 µg/ml in PBS) for 10 minutes. After washing several times in HBSS cells were treated with blocking buffer for one hour. The primary antibodies for Orco and Or22a (kindly donated by Leslie Vosshall) were diluted in blocking buffer having the recommended concentration and incubated at 4°C overnight. Three washing steps with PBS followed and the secondary antibody rabbit-alexa488 was added and incubated at room temperature for 2 hours. The cells were washed and the cover slips were mounted on slides using VectorShield mounting liquid. The staining was studied with the confocal microscope cLSM510 from Zeiss.

3. Results

3.1. Comparison of ionotropic and metabotropic current in Orco GYG transfected HEK-cells

To specify the number of pores in the OrX/Orco complex Orco GYG was exchanged for Orco wild type receptor protein. Orco GYG mutant was coexpressed with Or22a to check if the change in its ion permeability in regard to Orco would solely have an influence on the metabotropic response or on both. Following the protocol, recordings were acquired in HEK cells expressing Or22a and Orco GYG; thereby the loop was performed dependent on the duration of the response (Figure 5A). Etb (100nM) was applied for 2s and responses with an ionotropic and metabotropic component could be evoked (Figure 5B). An outward rectification was seen for the ionotropic response, which is typical for the dimer Orco/Or22a (Figure 5C, top). The metabotropic current showed a characteristic inward rectification as described for activation of mutant Orco GYG (Figure 5C, bottom).

To quantify the results the degree of rectification for ionotropic and metabotropic response was compared with Orco wild type experiments (Figure 5D). The degree of rectification for the ionotropic response in cells expressing Or22a and GYG (second light green column) is comparable to values for the ionotropic current in HEK cells transfected with Orco and Or22a (first red column). The degree of rectification of the ionotropic component is similar to the metabotropic one (second red column). Considering Orco and Orco GYG expressed alone, they show a notable difference caused by the changed ion permeability of Orco GYG (third and fourth column). The experiments with Or22a/Orco GYG reveal a similar degree of rectification in metabotropic response like the Orco GYG alone. So the receptor complex with Orco GYG retains the ability to produce an ionotropic and a metabotropic current; but only the metabotropic response changed characteristically regarding the rectification. This indicates that the OrX/Orco complex is comprised of two different pores, which open while ionotropic and metabotropic response.

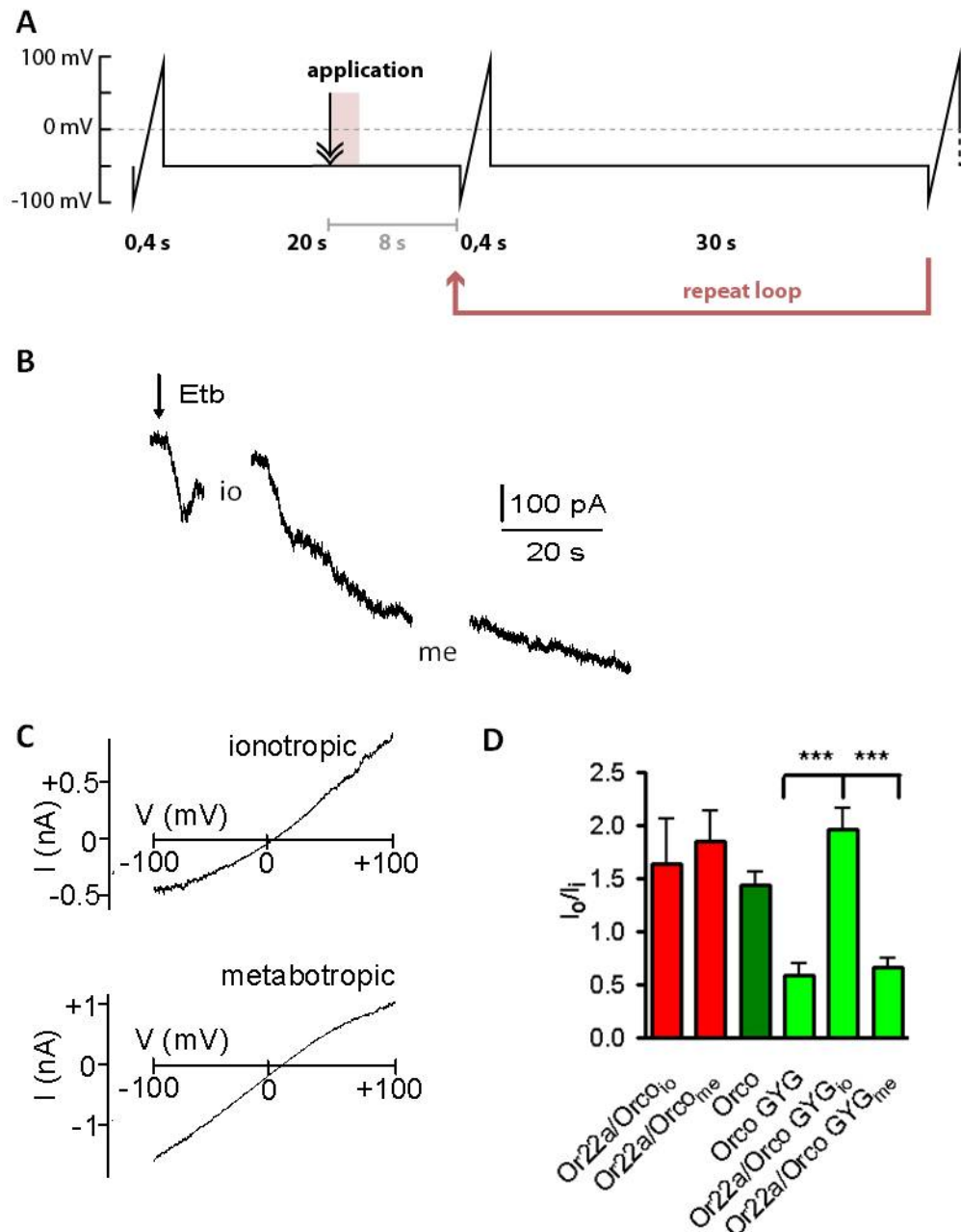


Figure 5 Etb induced currents for an Or22a/Orco GYG transfected HEK-cell in whole-cell configuration. **A** Protocol: After 12 s Etb (100 nM) was applied for 2 s (arrow), ramps (± 100 mV in 400 ms) and clamping at -50 mV for 30 s alternated until response ended. **B** Current in HEK293 cells transfected with Or22a/Orco GYG, activated by Etb (100 nM), 2 s application, (arrow) **C** ramp voltage protocols for ionotropic (io) and metabotropic (me) response, measured at the interruption of the corresponding recording in B (control currents subtracted). **D** Degree of current rectification (ratios of absolute values for currents at +100 mV and -100 mV) of wild-type and mutant channels in the given combination activated by Etb (Or22a/Orco and Or22a/Orco GYG) respectively 8-bromo-cAMP (Orco and Orco GYG). ***, $P < 0.001$; Student's t-test (Orco GYG/Or22a $n = 15$, other $n = 8$).

3.2 Permeability ratios for Orco PKC

To check whether PKC mutation affects the ion permeability voltage ramps (from -100 to +100 mV) were performed after stimulating with 8-bromo-cAMP. Current responses of Orco and Orco PKC are similar in its reversal potentials for whole-cell configuration (Sargsyan et al 2011). To determine ion selectivity of Orco PKC and Orco, the standard bath solution was exchanged with Ca^{2+} -free and Na^{+} -free solution. Channel opening was evoked by 8-bromo-cAMP, while running the protocol shown in Figure 1A. The permeability for Orco PKC amounts to $P_{\text{Na}}:P_{\text{K}} = 1.4 \pm 0.2$ for a Ca^{2+} -free solution ($n = 6$) and for a Na^{+} -free solution $P_{\text{Ca}}:P_{\text{K}} = 5.5 \pm 0.7$ ($n = 5$) resulting in a permeability sequence $P_{\text{Ca}}:P_{\text{Na}}:P_{\text{K}} = 5.5:1.4:1$. The found permeability ratios for Orco wild type are $P_{\text{Na}}:P_{\text{K}} = 1.1 \pm 0.3$, $P_{\text{Ca}}:P_{\text{K}} = 5.4 \pm 0.5$ and permeability sequence $P_{\text{Ca}}:P_{\text{Na}}:P_{\text{K}} = 5.4:1.1:1$ (Wicher et al 2008). The determined permeability ratios of Orco PKC for sodium and calcium are statistically not significantly different to those of Orco wild type (calculated by unpaired T-test; for $P_{\text{Na}}:P_{\text{K}}$: $p = 0.618$; $n_1 = 6$, $n_2 = 7$; for $P_{\text{Ca}}:P_{\text{K}}$: $p = 0.775$, $n_1 = 6$, $n_2 = 7$). Thus ion channels Orco and Orco PKC shape a pore with comparable ion selectivity.

3.3 Orco single channel currents

3.3.1 Determination of single-channel currents via amplitude histograms

Heterologous expressed Orco is activated directly by cAMP or cGMP. Current production indicates that the chaperoning co-receptor Orco can also function as channel (Wicher et al 2008). Single channel events could not be resolved in cells with a transient transfection (Sargsyan et al 2011), A transient transfection with Orco DNA leads to high expression levels and an increased incorporation into the cell membrane. Due to constitutive activity of Orco, a continuous Ca-influx stresses the cells. Calcium overload damages the cell, which is reflected in a changed physical appearance, thus cells are rounded. To avoid high expression a stable transfection was carried out in T-Rex cells. This is based on the idea

that only cells survive, in which the expression is low and thus the harmful effects of the constitutively active Orco are restricted. Because of this lower expression level a greater chance to observe single channel currents was assumed and a stable transfection in T-Rex cells was selected. In inside-out patches a certain constitutive activity was observed, but with application of cAMP the channel openings increased considerably. After stimulating with cAMP a response was observed after a few seconds (Figure 6A). Clear current steps in the recordings allow the determination of current level by using an all-point histogram. For an amplitude histogram all data points of the current trace were counted and the resulting number displayed in dependence on the current. This graph was fitted by Gaussian distribution and local maxima indicate abundant current level (Figure 6B). For an amplitude histogram all data points of the current trace were counted and the resulting number displayed in dependence on the current. This graph was fitted by Gaussian distribution and local maxima indicate abundant current level (Figure 6B).

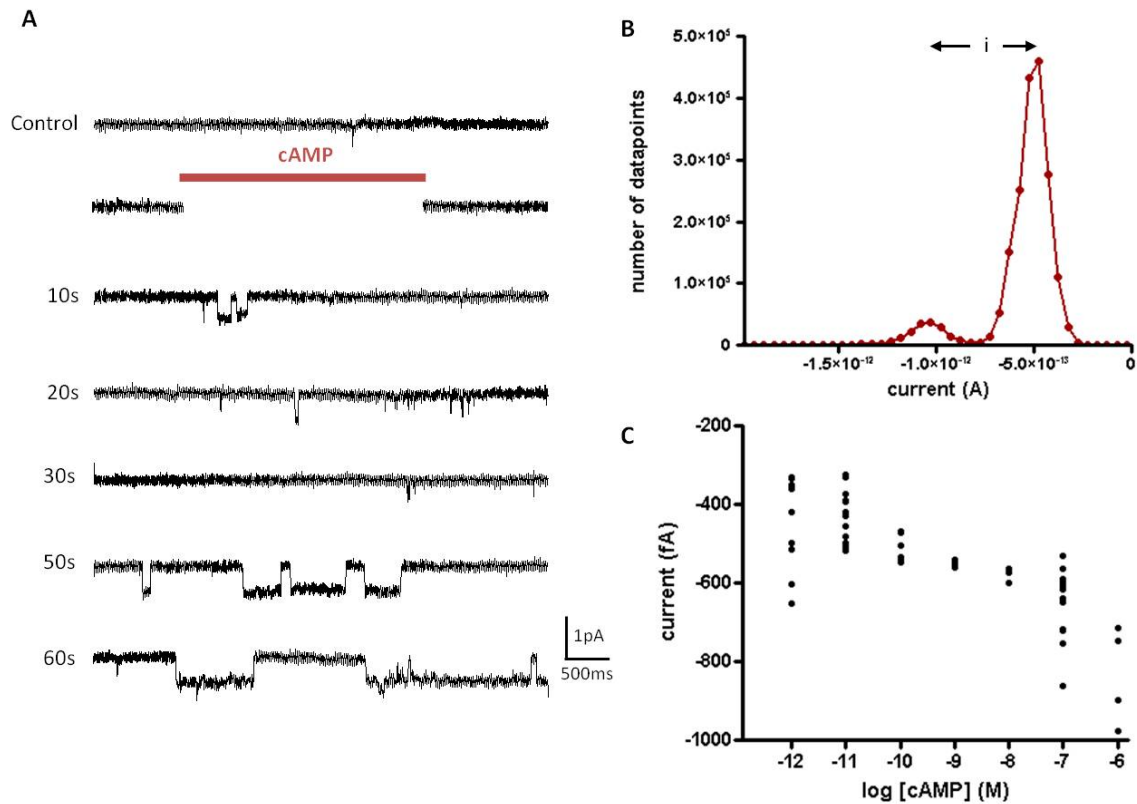


Figure 6 cAMP evoked currents in inside-out patches of T-Rex-cells stably expressing Orco. **A** Trace for an inside-out patch, holding potential at -50mV. Traces before stimulation with cAMP were used as control (digitally filtered by non-lagging Gaussian low-pass filter at 100Hz). **B** Amplitude histogram for the recording, from which sample traces were shown in A. Distance between local maxima (i) corresponds to distinct current steps. **C** Distinct current levels dependent on cAMP-concentration in this sample recording.

The distance between these local maxima (i, Figure 6B) correspond to current steps. Via this method current level were analyzed in dependence on the cAMP concentration (Figure 6C). Abundant current levels were uniform and constant within a certain time period in a recording. Their current distance was constant, thus there exist distinct steps, like demonstrated in Figure 6A. Distinct steps were seen in the majority of recordings, but the quantification of these levels is varying. The step size was constant for one patch, and furthermore clear steps and its multiples were observed and computed (Figure 7A). But these stable steps were only observed in a few cases; most of the recordings show more irregular currents at higher concentrations.

The smallest current steps measured in traces are ~ 50 fA; this corresponds to a conductance of 0.83 pS. Smaller current steps are hardly resolvable resulting from the given noise. Via the analysis with amplitude histograms current steps were computed to 30 fA (Figure 7C). A distinct and in different recordings frequently measured level is around 200 fA, as shown in Figure 7B. After pooling current steps at low cAMP concentration of all patches they resulted in a continuum (Figure 7C). Current steps varied between patches, indicating that an uniform conductance for one single channel is lacking (average current $I = 195,3 \pm 93,9$ fA; average conductance $3,3 \pm 1,6$ pS). As the cAMP response appears only delayed, endogenous currents can not be excluded in order to an ambiguous correlation between application and response.

3.3.2 Determination of single-channel currents via variance analysis

As an alternative to amplitude histograms the variance of non-filtered data can be used to determine single channel currents, even for recordings without resolvable current levels (Figure 8A, lower trace). The use of variance analysis is based on the fact that the variance changes according to the number of channel openings. Open channel increase the current hence the mean current is a measure for it. Variance reaches maximum, when 50% of the channels are open. In relation to the mean current this results in a parabolic shaped graph (Figure 8B).

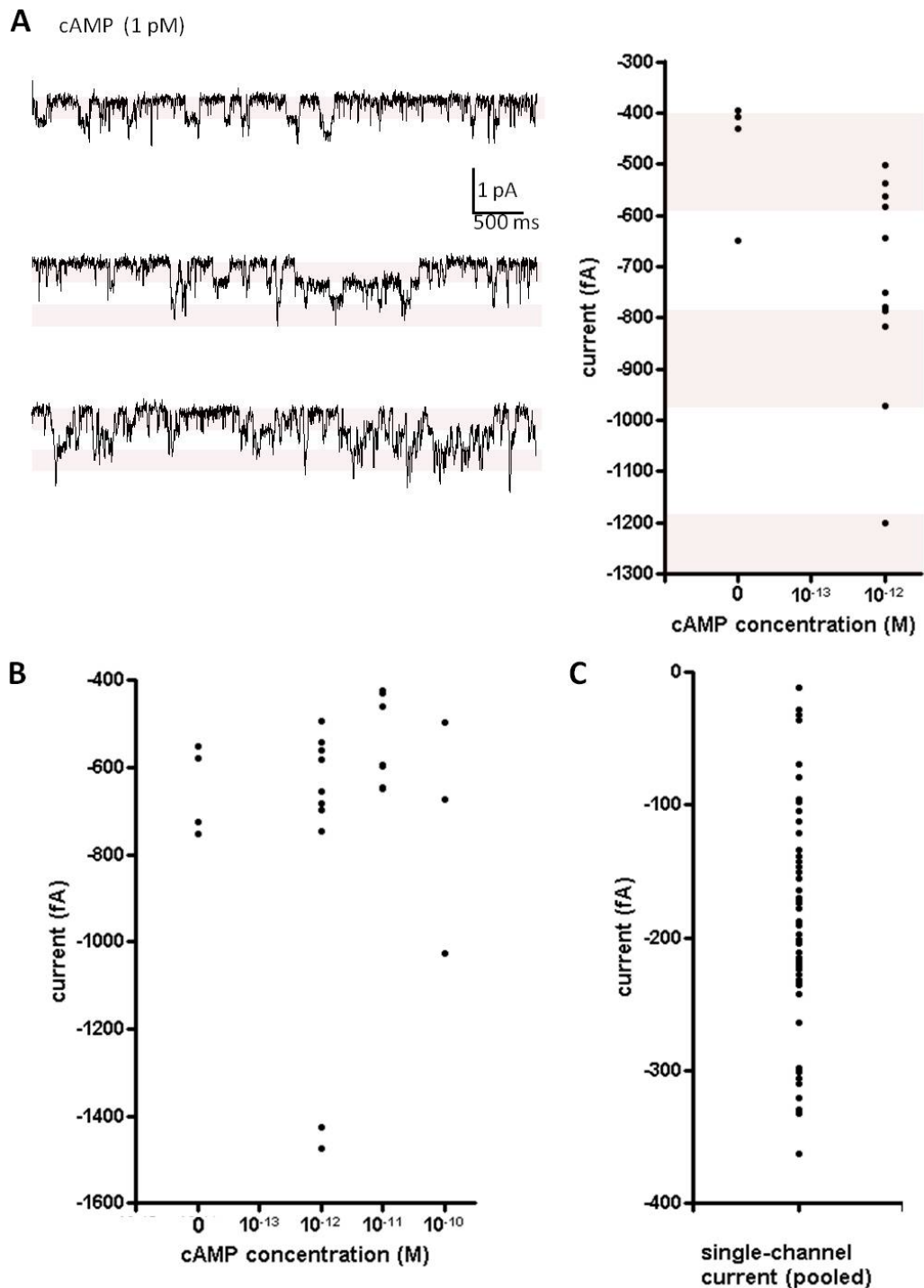


Figure 7 Characterization of single channel recordings by amplitude histogram method **A** Sample traces with multiple current steps, acquired in inside-out-configuration after applying 1 pM cAMP and corresponding single channel determination of the entire recording. **B** Analysis of a sample recording with distinct current steps in the range of 200 fA, level was stable for several concentration increases **C** Pooled single-channel currents for all recordings, calculated by amplitude histogram method (average current $I = 195,3 \pm 93,9$ fA).

The single channel current is determined by the slope at the origin of the variance-mean current curve. Variance is determined from non-filtered data and the slope of the tangent is computed (Figure 8C). To compare the lowest current steps only traces with single events (like shown in Figure 6A) were taken into account; these steps occur in the beginning of the recordings. For this approach the values for single channel currents are in the same order of magnitude and resulted also in a continuum (Figure 8D). Results were more variable compared to the values gained by the help of amplitude histograms (average current 341 ± 235 fA; $n = 11$). Also small currents of 50 fA size were found. This method confirms the dimension of single channel currents calculated via amplitude histograms.

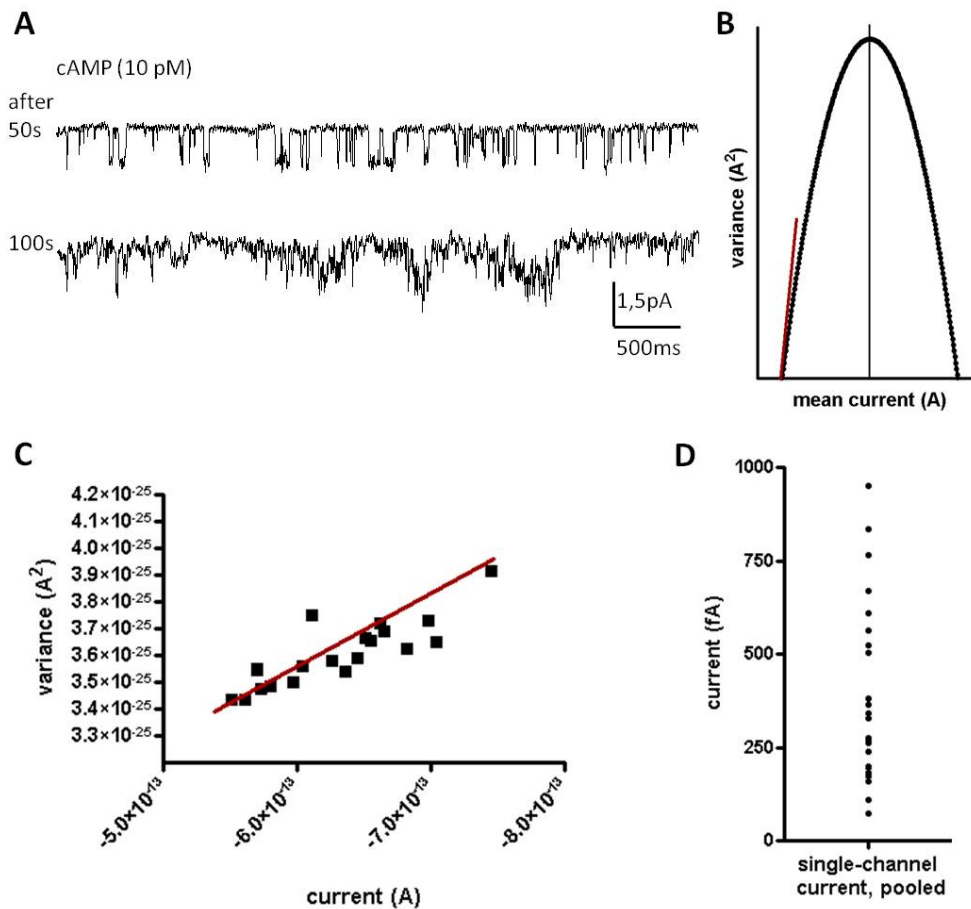


Figure 8 Single-channel currents calculated via variance analysis. **A** Distinct current steps were recorded (top); but also variable responses were (bottom). Data were digitally filtered by non-lagging Gaussian low-pass filter at 100Hz. **B** Schematic relationship between variance and mean current. Variance is maximal for a channel opening rate of 50 %. Red line displays the tangent at the origin of the graph. **C** Determination of single channel currents via the slope of tangent (first derivative, red line)

with measured variance in non-filtered recordings. **D** Pooled single-channel currents for all single current steps found in all recordings, quantified by analysis of variance method.

3.3.3. Concentration dependence

When applying higher concentration of cAMP the size of single current events rises (Figure 9A). For instance, the trace recorded for a 1 pM cAMP concentration shows small currents steps (~ 200 fA). At a concentration of 10 pM the current steps became larger (~ 1 pA); intermediate steps occur rarely.

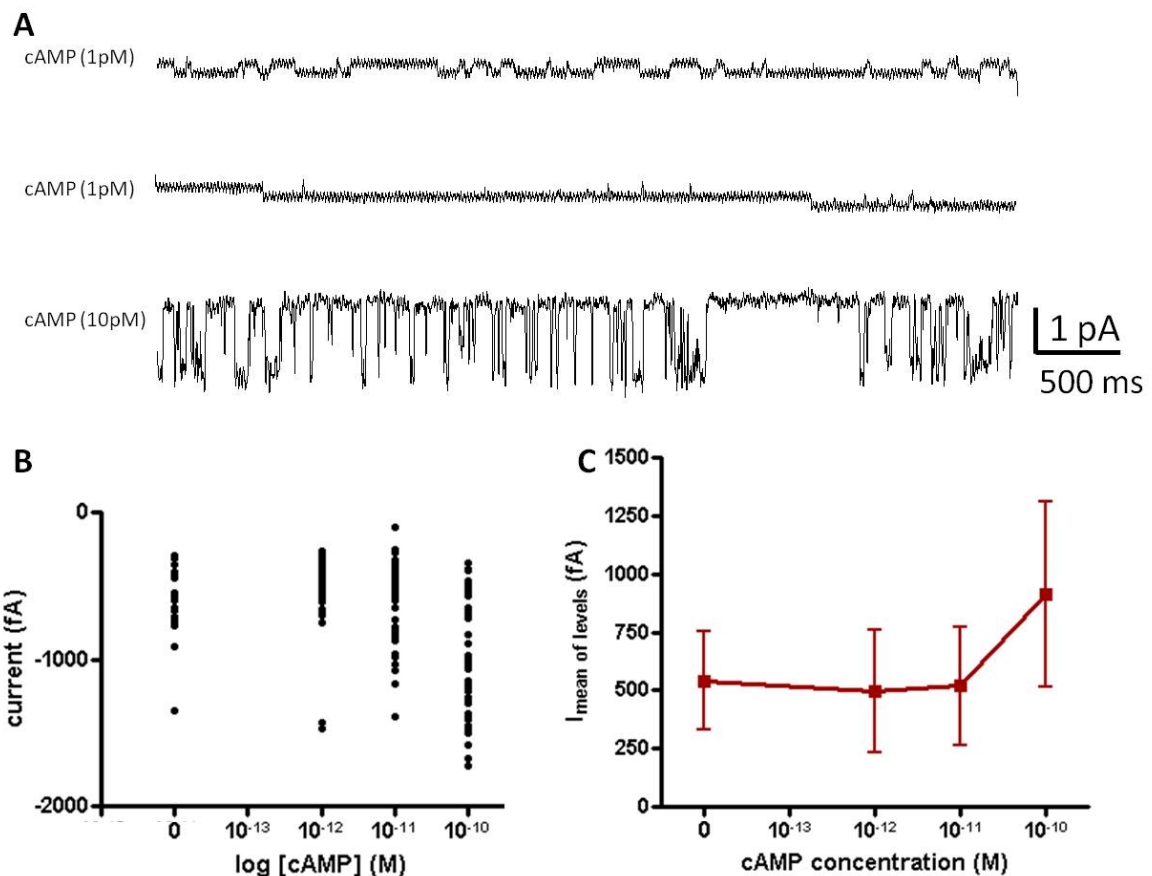


Figure 9 Concentration dependence for single channel recordings in T-Rex cells with a stable Orco expression. **A** Different traces within one sample recording (patches were clamped at -60 mV), describing a synchronized response at higher cAMP concentrations **B** Concentration dependent occurrence of current levels in inside-out recordings with T-Rex cells (stable expressing Orco) stimulated with cAMP from pooled data of all recordings ($n = 11$). **C** concentration-dependent curve with mean current level from pooled data shown in B, displayed as mean of current level.

At a given concentration short and long openings were observed (Fig. 9A top vs. middle). In this exemplarily trace the channel opening is continuous and a stepped increase of the current was observable. Taken together, there are distinct currents steps and they depend on the concentration of cAMP (compare Figure 7A). These enlarged currents (Fig. 9A bottom) may arise from cAMP dependence of single channel currents or by synchronized activity of several coreceptors.

Stimulation with various cAMP concentrations evokes larger current levels, clearly seen for single patches and pooled data ($n = 11$) from all patches (Figure 9B). Higher cAMP concentrations should cause a higher number of channels in the patch to open and hence additional current levels should emerge. A positive correlation between concentration and absolute values for current was determined. However, the stimulation with various concentrations differed with the recording, only two patches sustained for application with concentration higher than 10^{-10} M. Values for concentration higher than 10^{-10} M were excluded from the two recordings, because of the lacking stability in all patches. The resulting concentration-current curve displays a first correlation between cAMP-concentration and current for Orco stably expressed in T-Rex cells. A high sensitivity for concentrations at 10^{-10} M was found (Figure 9C).

3.4 Characterization of the transfection via immunofluorescence

3.4.1 Confocal micrographs

Cells transfected with Orco GYG/Or22a displayed rarely responses to Etb.. To check and quantify OR expression an immunohistochemical staining was carried out. A membrane staining was used to prove, if and to which extent transfected cells incorporate odorant receptor proteins into the membrane. Immunofluorescence of specific antibodies, tagging Or22a and Orco receptors, was matched with a membrane staining via conjugated wheat germ agglutinine (WGA). Confocal micrographs were gained by a multi-track scan with wavelength at 488 nm (for specific antibodies) and 543 nm (for WGA conjugated with TexasRed). The staining of Orco showed clear signals located in the membrane in cells

transfected with Orco and Or22a. The antibody against Orco can be used to tag Orco GYG, since the recognized epitopes are unchanged in this mutant. So stained cells showed co-localized signals for WGA conjugate and Orco GYG suggesting that Orco GYG is integrated into the membrane. Control experiments with non-transfected cells showed no specific staining, neither trials excluding the primary antibody (Figure 10A, B). To determine autofluorescence, transfected cells were treated without antibodies and showed no noticeable staining. In overview micrographs indicate that number of stained cells differs regarding the OR proteins. Cells stained against Or22a were not so abundant and clear outlined in relation to Orco or Orco GYG (Figure 10B-F). To examine the level of expression, fluorescence intensity profiles were compared, as described below.

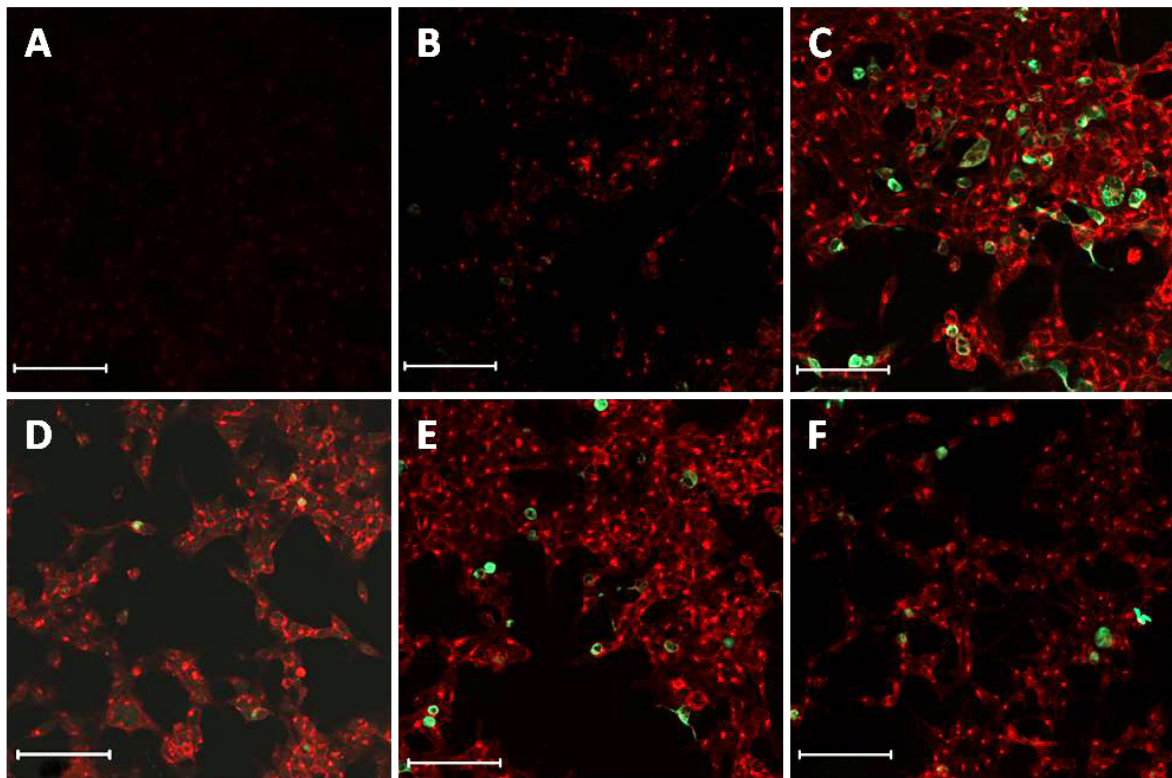


Figure 10 Confocal micrograph overviews taken for **A** non-transfected cells stained against Orco (control). **B-D** Confocal micrograph overviews for HEK293 cells transfected with Orco and Or22a and treated only with second antibody (**B**) stained against Orco (**C**) stained against Or22a (**D**). **E, F** Confocal micrograph overviews for HEK293 cells transfected with Orco GYG and Or22a and treated with primary antibody for Orco (**E**) stained against Or22a (**F**). Green, immunofluorescence; red, Texas-red fluorescence of wheat germ agglutinin (WGA) labeled plasma membrane; white bar 100 μM .

3.4.2 Membrane insertion of OR proteins

The highest transfection rate was seen for immunostaining against wild type Orco (WT) in HEK293 cells transfected with Orco and Or22a. The detected transfection rate for Or22a seems to be quite low. The averaged transfection rates were below 3% (Table 1). All cells irrespective of its physiological appearance were taken into account for this quantification.

Table 1 Expression rate (proportion of stained to all cells) for different transient transfections in HEK293-cells.

transfection	antibodies against	staining rate in %
Orco/22a	Orco	11.5
GYG/22a	Orco	6.4
Orco/22a	Or22a	1.8
GYG/22a	Or22a	2.6

Via a multi-track scan a colocalization of membrane staining with Orco and also Orco-GYG can be demonstrated in intensity profiles (Figure 11). Intensity profiles were compared to consider transfection levels of Or22a depending on the expressed co-receptor as a reason for sparse patch success. Confocal micrograph settings were retained for all acquisitions and the fluorescence signals were related to WGA fluorescence signals. The ratio of fluorescence intensity for Or22a and WGA signals is 0.83 ± 0.35 ($n = 6$) in GYG/Or22a transfected cells and 0.86 ± 0.14 ($n = 6$) for Orco/Or22a transfected cells; they showed no difference (Student's T-Test: $p = 0.79$). Nevertheless, intensity profiles supply clear evidence for a colocalization of fluorescence signals. Expression rate and transfection level are similar for Orco and Orco GYG, hence it seems they have a minor impact on the rare response to ETB in Orco GYG/Or22a cells. However a physiological difference of stained cells was observed. Tagged cells expressing Orco GYG and Or22a were more rounded and not in a good shape indicating to be more damaged. According to visual inspection of physiology Orco transfected cells showed a higher percentage of stained and healthy cells for coexpression with Or22a.

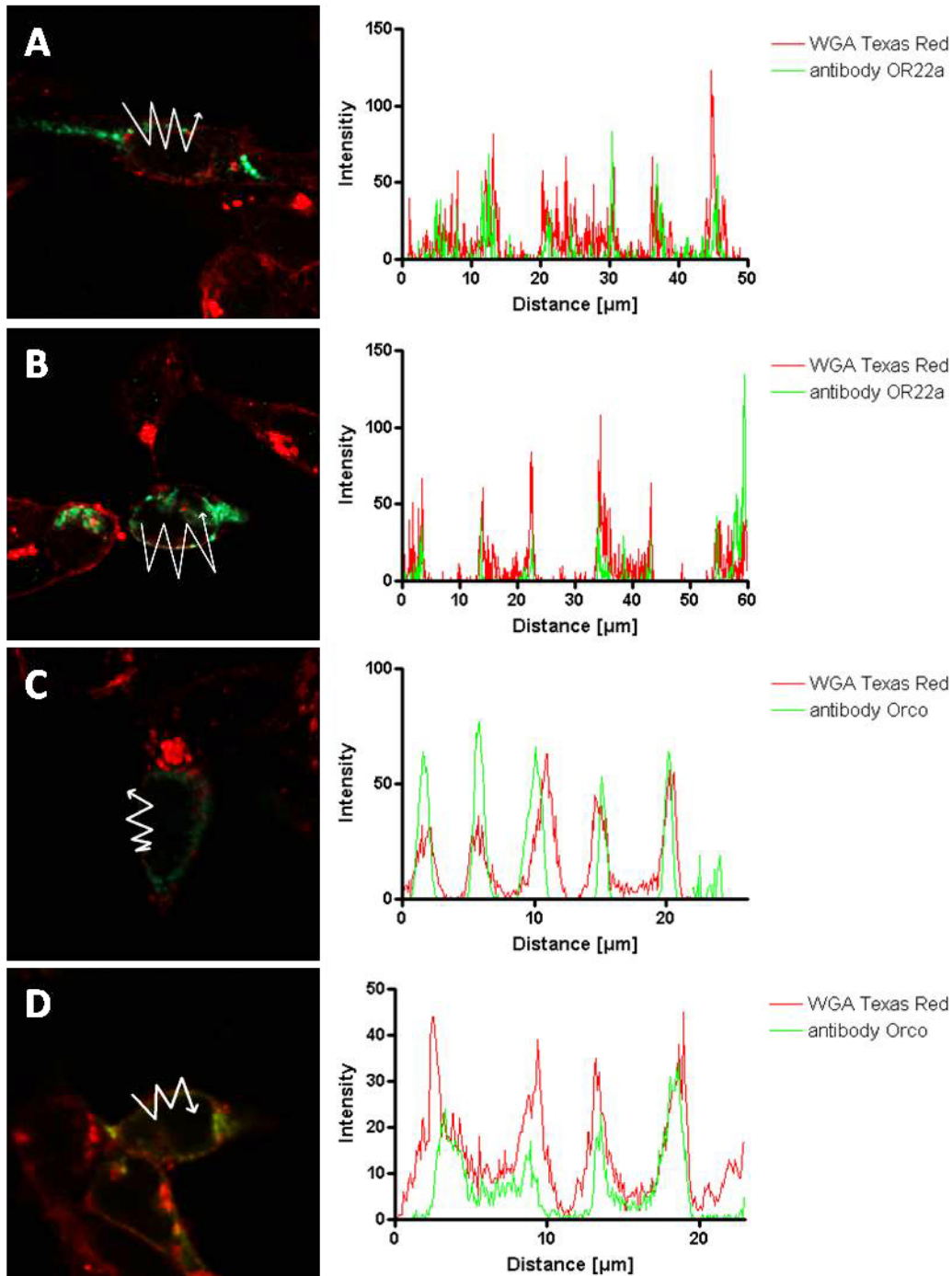


Figure 11 Confocal micrographs and fluorescence intensity profiles for HEK cells transfected **A** with Orco and Or22a and stained against Or22a **B** with Orco GYG and Or22a and stained against Or22a **C** with Orco and Or22a and stained against Orco **D** with Orco GYG and Or22a and stained against Orco. Green, immunofluorescence; red, Texas-red fluorescence of wheat germ agglutinine (WGA) labeled plasma membrane. White lines indicate position of intensity profiles given in the right column.

The transfection rate for healthy cells is five times higher than for Orco GYG transfected cells (Table 2). This reflects the deteriorated feasibility in patch-clamp-experiments, since only cells with a good physiology are chosen for experiments.

Table 2 Transfection rates for HEK-cells co-expressing Or22a and GYG or Orco were counted. An additional distinction compared to cell shape was made.

transfection	staining rate in %	stained and good-shaped in %
Orco/22a	1.8	24.5
GYG/22a	2.6	4.9

4. Discussion

4.1. Insect ORs form two pore channels

To determine the number of pores in the receptor complex Orco GYG and Or22a were coexpressed in HEK293 cells and stimulated with Etb. Iontropic current ramps had a similar rectification considering the receptor complex with Orco wild type, whereas the metabotropic response has shown different properties compared to wild type Orco. The metabotropic response showed an inward rectification, in order to the reduced K⁺ permeability of Orco GYG mutant. This result supports the assumption that the OrX/Orco complex can form two different pores. This finding provides evidence for a transduction model with two different pores shaped while ionotropic and metabotropic response. One pore is thought to be built by Orco and the according conventional receptor, the other pore is merely formed by Orco. The assumption that Orco forms a pore alone is supported by the fact that Orco produces currents in HEK cells without any conventional ligand binding receptor (Wicher et al 2008). Moreover, currents could be generated with the recently discovered agonist VUAA1 in cells, in which only Orco of various insects has been expressed. A configuration of two pores is conceivable considering the voltage-gated proton channel Hv1, which forms a dimer of four transmembrane segments and shapes two pores. But even without dimerization conductivity was demonstrated for Hv1 monomers, suggesting that each monomer has one pore (Chatterjee et al 2009). In a recent study a 6-Å projection map of the light-gated ion channel Channelrhodopsin-2 reveals the structure of a pore shaped by two 7-transmembrane monomers. The ChR2 pore is located at the dimer interface on the 2-fold axis, lined by transmembrane helices 3 and 4 (Müller et al 2011). This illustrates an option, how a pore might be shaped by two Orco monomers.

The results of Sato et al, who found an ionotropic response without G-proteins (Sato et al 2008), confirm the finding of another pore, which is conceivably responsible for the rapid signal generation. Furthermore, it has been found that current response was dependent on the specificity of the two subunits together. Orco was coexpressed with various

conventional receptors and one conventional receptor with various Orco types from different species. However, Orco had no effect on responding to the conventional profile of the receptor to specific ligands (Nichols et al 2011). Thus, the current response of one pore depends on the matching of the receptor proteins.

Thus far it is unknown, which parts of the involved proteins are shaping the channels and also the location of the channel pore built by OrX/Orco is not specified until now.

4.2 PKC mediated phosphorylation does not affect Orco permeability

Orco as part of the metabotropic pathway might be subject regulatory mechanisms via G_q proteins: It was demonstrated that Orco is modulated via PKC, which is dependent on G_q proteins and Ca^{2+} concentration: Recent experiments showed that an inhibition of PLC reduces the sensitivity of Orco to cAMP. In addition a microinjection of PLC and PKC inhibitors into sensilla reduces the response of odorant sensory neurons. Through mutation of phosphorylation sites in Orco a reduction in cAMP sensitivity was affected (Sargsyan et al 2011). In that experiment three different mutants were used, which differ in the number of altered phosphorylation sites. In the present work the Orco PKC mutant with five and thus the most changes was taken to determine its ion permeability. The results in the present study showed similar ion permeability as Orco wild type. Thus, the observed reduction in the response to cAMP in the paper by Sargsyan et al is not due ion permeability of Orco PKC. This confirms the thesis that the state of phosphorylation of Orco has an influence on the function of Orco.

4.3 Orco single channel current

Pursuing the characterization of Orco the single conductance for Orco was tried to be determined in this work. Determination of single channel currents produced variable results and a uniform single channel current for one Orco channel is lacking, instead the values for single currents revealed a continuum with an average current around 200 fA.

Besides the continuum among the patches a characteristic pattern was observed within many recordings. The response to higher concentrations seems to occur as multiples of the distinct steps for lower concentrations. Thereby the higher excitation levels are reached in steps or at once, thus synchronized. In the beginning of the only little distinct levels emerged, though in the course of the experiments these steps were enhanced at a multiple of the initial niveau. Noteworthy is a presumably concurrency of the enhanced response. The odorant coreceptors appear to be linked for a synchronized response. Difficulties to obtain a single channel current and similar synchronized responses were reported in patch-clamp experiments on sugar receptor cells of the blow fly (Kan et al 2008). The question, how these larger currents are caused, needs further investigation. On the one hand cAMP could induce a conformational change in Orco, which could affect the conductance for a channel. On the other hand an association of Orco monomers could cause a temporally coupled response of several coreceptors. But how openings of Orco could link together for a simultaneous response is unknown. Also a pore formed by several monomers is conceivable and the number of involved receptors could determine the conductance of the pore, like described for Alamethicin. This antibiotic with various conductance levels is suggested to build pores composed of 3-12 monomers; whereas the number of monomers is correlated with the conductance of the channel (Leitgeb et al 2007).

Recently VUAA1 was found to act as agonist for the Orco family. VUAA1 raised instantly currents in HEK293 cells expressing the *Anopheles gambiae* coreceptor (AgOrco) and other orthologues (Jones et al 2011). The study of Jones et al. reports single channel currents for AgOrco ($I = 1,3 \text{ pA}$), these are notably higher compared to the found results in this work. Jones et al. used a transient transfection in HEK293 cells, which could lead to a higher expression of Orco and therefore higher currents. Moreover, it can be assumed that the synchronicity of Orco monomers is facilitated by a higher expression of Orco. However, in the present work higher cAMP concentration evoked currents with a similar magnitude and appearance (as shown in Figure 9A, lower trace). So reasons and mechanism for the synchronization of Orco have to be elaborated. It can be speculated, that cAMP is involved in an association of Orco and leads to synchronized activity, but this needs further investigation.

Even with a fast application the stimulus response of cAMP is delayed and so an endogenous reaction while inside-out recordings can not be excluded. For a clearer correlation of stimulus and response further experiments are needed. Perspective inside-out recordings with VUAA1 should evoke stimulus correlated currents with the result of a more revealing single conductance determination.

4.4 Current model of insect olfactory receptor signal transduction

The current results are summarized in the following model of the olfactory signal transduction in *D. melanogaster*: To perceive odors an appropriate ligand binds to the conventional receptor, for Or22a e. g. ethyl butyrate (Etb). This causes an ionotropic current in interaction with the ubiquitous coreceptor Orco.

Through activation of the conventional receptor $G_s\alpha$ subunits are released, which stimulate the adenylyl cyclase. Adenylyl cyclase converts ATP into cAMP. By rising cAMP levels Orco is activated and metabotropic currents are induced. The response of Orco is dependent on G_q proteins signaling cascades, although the basic activity of the enzymes PLC and PKC is sufficient for the activity of Orco. Both PKC and PLC affect the sensitivity of Orco (Sargsyan et al 2011). The PLC is activated by G_q proteins and hydrolyse PIP_2 into IP_3 and DAG. The released DAG activates the PKC, which phosphorylates Orco and hereby regulates its function. Beside DAG a minimum intracellular Ca^{2+} concentration is required for activity of PKC (Figure 12).

In sum an involvement of G_s and G_q proteins were proven in metabotropic pathway (Kain et al 2008, Wicher et al 2008), the suggested model from Nakagawa and Vosshall takes $G_{i/o}$ proteins into account for the regulation of Orco. Recent study showed that inhibition of G_o proteins by pertussis toxin reduced responses evoked by ethyl acetate (Chatterjee et al 2009). This provides evidence that G_o proteins is required for maximal physiological responses to odors. Until now it remains to be elucidated, if there are G_i proteins are also involved in olfactory pathways.

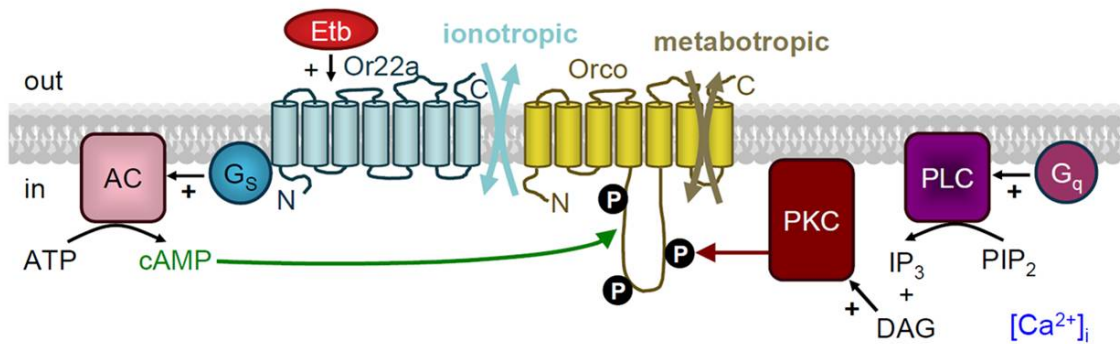


Figure 12 Model of odorant signaling pathways: Through the odor stimulation (e.g. Etb) the conventional receptor Or22a induces the ionotropic pathway (light blue arrows), the emerging ion channel opens fast and transient. Coincident Or22a activates G_s proteins, which trigger adenylyl cyclase leading to an increased cAMP level. As a result Orco and thereby the metabotropic response is activated. Orco sensitivity is modulated by PKC-mediated Orco phosphorylation. The relation between Orco and Or22a is unknown currently. Abbreviations: Etb, ethyl butyrate; AC, adenylyl cyclase; P phosphorylation site; PKC, protein kinase C; DAG, diacylglycerol; IP_3 , inositol 1,4,5-trisphosphate; PIP_2 phosphatidylinositol 4,5-bisphosphate; PLC, phospholipase C.

In this work evidence was found, that the receptor complex forms two different pores. How these channels are linked to each other in olfactory transduction and how do they influences this response? It is expected that the conventional receptor activation determines the activity of Orco via G_s proteins. On the other hand it is assumed that Orco feeds back the activity of the conventional receptor. In addition, a signal cascade via G_q proteins enables a regulation of the OrX/Orco complex independent of odor induced mechanisms (Sargsyan et al 2011). Based on this, it can be assumed that there are regulation mechanisms for the ionotropic response without any odorant signaling caused by a ligand and its matching conventional receptor.

5. Summary

The patch-clamp technique was performed to investigate the properties and function of the OrX/Orco complex of *Drosophila melanogaster*. For the determination of the pore involved in signal formation the response of Or22a/Orco complex to the matching odorant Etb was compared to the response of Orco GYG mutant and Or22a on Etb. The resulting currents after stimulation showed a change in rectification only for the metabotropic response and thus suggest that the complex is able to form two distinct pores.

The determined permeability ratios for Orco PKC mutants support the finding of a decreased cAMP sensitivity of Orco PKC (Sargsyan et al 2011). Since no significant changes in permeability compared to wild type were found, the decreased response of Orco PKC is not owed to a changed permeability.

While single-channel current determination of Orco a distinct single channel current was not found, there were variable but distinct steps in channel opening for inside-out patches after stimulation with low concentration of cAMP. For future experiments it would be interesting to understand the finding of a variable conductance of the Orco channel pore. Further investigation is needed to understand the mechanisms and mutual influence of the subunits of the OrX/Orco complex as well as the manifestation of the metabotropic components.

6. Acknowledgements

I would like to express my appreciation to PD Dr. Dieter Wicher for introducing me to insect olfaction and for his guidance through the hitherto for me untouched sphere of electrophysiology.

Further I thank Prof. Dr. Bill S. Hansson for giving me the opportunity to accomplish my work at the Max-Planck-Institute for Chemical Ecology.

Especially I want to thank Nico Funk for supporting me and brighten up the daily routine in the “patchlab” as well as Regina Stieber, Anna Kretschmar, Veit Grabe, Antonia Strutz, Vardanush Sargsyan and the complete evolutionary neuroethology group in Jena for their help, the discussions and for making the work in the institute such pleasant. For taking care of cell culture and preparing all these cell dishes I want to thank Sabine Kaltofen and Sylke Dietel.

Finally I give thanks to my beloved father - for his support and implicit trust at all times and especially during my thesis.

7. References

- Benton R, Sachse S, Michnick SW, Vosshall LB. 2006. Atypical membrane topology and heteromeric function of *Drosophila* odorant receptors in vivo. *PLoS Biol* 4: e20
- Benton R, Vannice KS, Gomez-Diaz C, Vosshall LB. 2009. Variant ionotropic glutamate receptors as chemosensory receptors in *Drosophila*. *Cell* 136: 149-62
- Carey AF, Carlson JR. 2011. Insect olfaction from model systems to disease control. *Proc. Natl. Acad. Sci. U.S.A.* 108: 12987-95
- Chatterjee A, Roman G, Hardin PE. 2009. G(o) contributes to olfactory reception in *Drosophila melanogaster*. *BMC Physiol.* 9: 22
- Clyne PJ, Warr CG, Freeman MR, Lessing D, Kim JH, Carlson JR. 1999. A novel family of divergent seven-transmembrane proteins: Candidate odorant receptors in *Drosophila*. *Neuron* 22: 327-38
- Couto A, Alenius M, Dickson BJ. 2005. Molecular, anatomical, and functional organization of the *Drosophila* olfactory system. *Curr. Biol.* 15: 1535-47
- Deng YDY, Zhang WY, Farhat K, Oberland S, Gisselmann G, Neuhaus EM. 2011. The Stimulatory G alpha(s) Protein Is Involved in Olfactory Signal Transduction in *Drosophila*. *PLoS One* 6
- Elmore T, Ignell R, Carlson JR, Smith DP. 2003. Targeted mutation of a *Drosophila* odor receptor defines receptor requirement in a novel class of sensillum. *J. Neurosci.* 23: 9906-12
- Gao Q, Chess A. 1999. Identification of candidate *Drosophila* olfactory receptors from genomic DNA sequence. *Genomics* 60: 31-39
- Gao Q, Yuan BB, Chess A. 2000. Convergent projections of *Drosophila* olfactory neurons to specific glomeruli in the antennal lobe. *Nat. Neurosci.* 3: 780-85
- Grimaldi D, Engel MS. 2005. *Evolution of the insects*. Cambridge University Press. i-xv, 1-755 pp.
- Hamill OP, Marty A, Neher E, Sakmann B, Sigworth FJ. 1981. Improved patch-clamp techniques for high-resolution current recording from cells and cell-free membrane patches. *Pfluegers Arch.* 391: 85-100
- Heisenberg M. 1998. What do the mushroom bodies do for the insect brain? An introduction. *Learn. Memory* 5: 1-10
- Hodgkin AL, Huxley AF. 1952. A quantitative description of membrane current and its application to conduction and excitation in nerve. *J. Physiol.* 117: 500-44

- Jones PL, Pask GM, Rinker DC, Zwiebel LJ. 2011. Functional agonism of insect odorant receptor ion channels. *Proc. Natl. Acad. Sci. U.S.A.* 108: 8821-25
- Kain P, Chakraborty TS, Sundaram S, Siddiqi O, Rodrigues V, Hasan G. 2008. Reduced odor responses from antennal neurons of G(q)alpha, phospholipase Cbeta, and rdgA mutants in *Drosophila* support a role for a phospholipid intermediate in insect olfactory transduction. *J. Neurosci.* 28: 4745-55
- Kan H, Kataoka-Shirasugi N, Amakawa T. 2008. Transduction pathways mediated by second messengers including cAMP in the sugar receptor cell of the blow fly: Study by the whole cell clamp method. *J. Insect Physiol.* 54: 1028-34
- Krieger J, Klink O, Mohl C, Raming K, Breer H. 2003. A candidate olfactory receptor subtype highly conserved across different insect orders. *J. Comp. Physiol. [A]* 189: 519-26
- Larsson MC, Domingos AI, Jones WD, Chiappe ME, Amrein H, Vosshall LB. 2004. Or83b encodes a broadly expressed odorant receptor essential for *Drosophila* olfaction. *Neuron* 43: 703-14
- Leitgeb B, Szekeres A, Manczinger L, Vagvolgyi C, Kredics L. 2007. The history of alamethicin: A review of the most extensively studied peptaibol. *Chem. Biodivers.* 4: 1027-51
- Müller M, Bamann C, Bamberg E, Kühlbrandt W. 2011. Projection Structure of Channelrhodopsin-2 at 6 Å Resolution by Electron Crystallography. *J. Mol. Biol.* 414: 86-95
- Nakagawa T, Vosshall LB. 2009. Controversy and consensus: noncanonical signaling mechanisms in the insect olfactory system. *Curr. Opin. Neurobiol.* 19: 284-92
- Naresh Singh R, Nayak SV. 1985. Fine structure and primary sensory projections of sensilla on the maxillary palp of *Drosophila melanogaster* Meigen (Diptera : Drosophilidae). *Int. J. Insect Morphol. Embryol.* 14: 291-306
- Neuhaus EM, Gisselmann G, Zhang W, Dooley R, Stortkuhl K, Hatt H. 2005. Odorant receptor heterodimerization in the olfactory system of *Drosophila melanogaster*. *Nat. Neurosci.* 8: 15-7
- Nichols AS, Chen SS, Luetje CW. 2011. Subunit Contributions to Insect Olfactory Receptor Function: Channel Block and Odorant Recognition. *Chem. Senses* 36: 781-90
- Sargsyan V, Getahun MN, Lavista Llanos S, Olsson SB, Hansson BS, Wicher D. 2011. Phosphorylation via PKC regulates the function of the *Drosophila* odorant coreceptor. *Front. Cell. Neurosci.* 5
- Sato K, Pellegrino M, Nakagawa T, Vosshall LB, Touhara K. 2008. Insect olfactory receptors are heteromeric ligand-gated ion channels. *Nature* 452: 1002-6

- Shanbhag SR, Muller B, Steinbrecht RA. 1999. Atlas of olfactory organs of *Drosophila melanogaster* - 1. Types, external organization, innervation and distribution of olfactory sensilla. *Int. J. Insect Morphol. Embryol.* 28: 377-97
- Silbering AF, Rytz R, Grosjean Y, Abuin L, Ramdya P, et al. 2011. Complementary Function and Integrated Wiring of the Evolutionarily Distinct *Drosophila* Olfactory Subsystems. *J. Neurosci.* 31: 13357-75
- Strausfeld NJ, Hildebrand JG. 1999. Olfactory systems: common design, uncommon origins? *Curr. Opin. Neurobiol.* 9: 634-39
- Vogt RG, Riddiford LM. 1981. Pheromone binding and inactivation by moth antennae. *Nature* 293: 161-63
- Vosshall LB, Amrein H, Morozov PS, Rzhetsky A, Axel R. 1999. A spatial map of olfactory receptor expression in the *Drosophila* antenna. *Cell* 96: 725-36
- Vosshall LB, Stocker RE. 2007. Molecular architecture of smell and taste in *Drosophila*. In *Annu. Rev. Neurosci.*, pp. 505-33. Palo Alto: Annual Reviews
- Vosshall LB, Wong AM, Axel R. 2000. An olfactory sensory map in the fly brain. *Cell* 102: 147-59
- Wicher D, Schafer R, Bauernfeind R, Stensmyr MC, Heller R, et al. 2008. *Drosophila* odorant receptors are both ligand-gated and cyclic-nucleotide-activated cation channels. *Nature* 452: 1007-11
- Wilson RI, Laurent G. 2005. Role of GABAergic inhibition in shaping odor-evoked spatiotemporal patterns in the *Drosophila* antennal lobe. *J. Neurosci.* 25: 9069-79
- Yao CA, Carlson JR. 2010. Role of G-proteins in odor-sensing and CO₂-sensing neurons in *Drosophila*. *J. Neurosci.* 30: 4562-72
- Yao CA, Ignell R, Carlson JR. 2005. Chemosensory coding by neurons in the coeloconic sensilla of the *Drosophila* antenna. *J. Neurosci.* 25: 8359-67

8. List of abbreviations

AC	Adenylyl cyclase
AKHR	Adipokinetic hormone receptor
AL	Antennal lobe
ATP	Adenosine triphosphate
CaM	Calmodulin
cAMP	Cyclic adenosine monophosphate
cGMP	Cyclic guanosine monophosphate
CGN	Cyclic nucleotide-gated channel
DAG	Diacylglycerol
EGFP	Enhanced green fluorescent protein
EGTA	Ethylene glycol tetraacetic acid
Etb	Ethyl butyrate
FBS	Fetal bovine serum
GABA	γ -aminobutyric acid
GC	Guanylate cyclase
GDP- β S	Guanosine 5'-O-(2-thiodiphosphate)
GTP	Guanosine-5'-triphosphate
HCN	Hyperpolarization-activated cation channel
HEK	Human embryonic kidney
HEPES	N-[2-hydroxyethyl]piperazine-N'-[2-ethanesulfonic acid]
IP ₃	Inositol-1,4,5-triphosphate
OR	Odorant receptor
OSN	Olfactory sensory neuron
NMDG	N-methyl-D-glucamine
NGS	Normal goat serum
PBS	Phosphate buffered saline
PIP ₂	Phosphatidylinositol 4,5-bisphosphate
PKA	Protein kinase A
PKC	Protein kinase C

PKG	Protein kinase G
PLC	Phospholipase C
PTX	Pertussis toxin
RNA	Ribonucleic acid
Tris	Tris (hydroxymethyl)-aminomethan
VUAA	2-(4-ethyl-5-(pyridin-3-yl)-4H-1,2,4-triazol-3-ylthio)-N-(4-ethylphenyl)acetamide

9. Declaration of academic integrity

I hereby declare that the work submitted during the course of my degree is my own work. All parts of this assignment, which are contributions from other sources, are recognizable and clearly defined with their respective references. All submitted copies of this work are identical.

Jena, 11/30/2011

.....
Kerstin Pasemann